

## BRIEF COMMUNICATIONS

The purpose of this Brief Communications section is to present important research results of more limited scope than regular articles appearing in *Physics of Plasmas*. Submission of material of a peripheral or cursory nature is strongly discouraged. Brief Communications cannot exceed four printed pages in length, including space allowed for title, figures, tables, references, and an abstract limited to about 100 words.

### Laser-plasma diamagnetism in the presence of an ambient magnetized plasma

M. VanZeeland<sup>a)</sup> and W. Gekelman

*Department of Physics and Astronomy, University of California, Los Angeles, California 90095-1547*

(Received 13 August 2003; accepted 3 September 2003)

This work is an experimental study of the diamagnetic cavity created by a dense laser-produced plasma (initially,  $n_{\text{lpp}}/n_0 \gg 1$ ) expanding into an ambient magnetized background plasma ( $n_0 = 2 \times 10^{12} \text{ cm}^{-3}$ ) capable of supporting Alfvén waves. The experiments are carried out on the upgraded Large Plasma Device [W. Gekelman, H. Pfister, Z. Lucky, J. Bamber, D. Leneman, and J. Maggs, *Rev. Sci. Instrum.* **62**, 2875 (1991)] at UCLA. Two-dimensional data of both the diamagnetic cavity as well as visible light emission are presented and found to be rich in structure with spatially similar characteristics. Laser-plasma diamagnetism has been observed to be relatively unaffected by the presence of a background plasma for  $n_{\text{lpp}}/n_0 \approx 10$  at time of peak diamagnetism. © 2004 American Institute of Physics. [DOI: 10.1063/1.1628233]

Examples of high-beta plasmas embedded in ambient magnetized plasmas permeate all areas of plasma and astrophysics, i.e., supernova explosions, coronal mass ejections,<sup>1</sup> high-altitude nuclear explosions,<sup>2</sup> inertial confinement fusion plasmas,<sup>3–5</sup> and bolid impacts.<sup>6</sup> Previous experiments aimed at simulating these phenomena have used laser-produced plasmas (lpp) embedded in both ambient photo-ionized gas and a theta-pinch plasma.<sup>7–10</sup> Other experiments such as the Active Magnetospheric Particle Tracer Explorers and Combined Release and Radiation Effects Satellite used exploding canisters of barium which were detonated in the ionosphere. A common theme to each of these experiments was the formation and relaxation of a diamagnetic cavity.<sup>11,12</sup>

The experiment presented here centers on the use of a laser to generate rapidly expanding, dense plasmas embedded in an ambient background plasma. When a laser-produced plasma expands across a background magnetic field in vacuum it goes through several phases. The initial laser impact results in immediate ionization of surface atoms and a blast of fast electrons ( $E < 100 \text{ eV}$ ) which rip ions from the target surface due to a large ambipolar field. The more massive ions hold back the electrons and eventually overshoot them due to their relative unmagnetized state. This creates a radially inward directed ambipolar field which in turn causes an electron  $\mathbf{E} \times \mathbf{B}$  drift and, in conjunction with  $\nabla P \times \mathbf{B}$  currents, the observed laser-plasma diamagnetism.<sup>13</sup> The lpp diamagnetic cavity size can be approximated by setting the total excluded magnetic energy equal to the kinetic energy of the laser-plasma,  $E_{\text{lpp}}$ . Namely, a magnetic con-

finement or “bubble” radius  $R_b = (3\mu_0 E_{\text{lpp}}/2\pi B_0^2)^{1/3}$ .<sup>7,10,14</sup> Both the diamagnetic bubble scaling and ambipolar field have been observed in previous experiments where the expansion occurred into vacuum<sup>14</sup> and background gas.<sup>7,9,10</sup>

When a background plasma is present, lpp diamagnetism is complicated because the background electrons can shuttle along field lines and partially short out the initial large ambipolar field allowing laser-plasma electrons to escape consequently radiating shear Alfvén waves.<sup>15–17</sup> The experiment mentioned here is the first to carry out an investigation of the diamagnetic cavity formed by an expanding sub-Alfvénic laser-produced plasma embedded in an ambient magnetized background plasma for a variety of background plasma conditions in which the ambient plasma can support Alfvén waves. Shear Alfvén wave generation by an expanding lpp has been reported previously by this group.<sup>13,17,18</sup> Experiments have shown that shear Alfvén wave radiation into the background plasma may account for as much as 10% of the initial lpp kinetic energy. This combined with other effects such as compressional Alfvén wave generation and additional currents which can form in the ambient plasma may affect other facets of lpp dynamics<sup>19,20</sup> but have not been observed to significantly affect the diamagnetic cavity itself.

The measurements reported in this paper were taken on the upgraded Large Plasma Device.<sup>21</sup> The background plasmas in this experiment were neon or helium  $M_i = 20, 4$ ,  $n_0 = 2 \times 10^{12} \text{ cm}^{-3}$ ,  $T_e = 5 \text{ eV}$ ,  $T_i = 1 \text{ eV}$ , diam = 50 cm as determined by Langmuir probe measurements in a plane. The background magnetic field ( $B_0$ ) was varied from 0.5 to 1.5 kG and axially uniform. The laser used was a 1.5 J/pulse, 8 ns full-width half maximum, Q-switched Nd-Yag focussed to

<sup>a)</sup>Electronic mail: mav@physics.ucla.edu

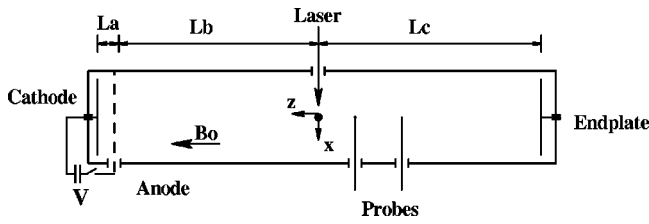


FIG. 1. A schematic of the experimental configuration.  $L_a=50$  cm,  $L_b=667$  cm,  $L_c=1033$  cm, plasma diameter=50 cm,  $B_o=0.5-1.5$  kG,  $V < 60$  V. The laser impacts the target surface at  $x=0, y=0, z=0$ .

an on-target spot diameter of 0.5 mm and is both temporally and spatially Gaussian shaped. The target, located 661.5 cm from the cathode, is a 1.9 cm diam aluminum or carbon rod which, to ensure a fresh target surface, is translated and/or rotated using a dual stepper motor system by 1 mm after every 5 shots. A diagram of the setup is shown in Fig. 1. The coordinate system used is centered at the laser impact point and is also shown in Fig. 1.

The probes used in this experiment are a single-turn magnetic pickup loop with an area of  $3.1 \text{ mm}^2$ , a 3-axis inductive pickup loop system and a fast gated imager ( $\tau_{\text{exp}} < 10$  ns). Each axis of the 3-axis magnetic probe consisted of a pair of 3-turn loops differentially wound to reduce electrostatic pickup. The total combined area of all six coils for each axis is  $0.835 \text{ cm}^2$ .

The experiment proceeds as follows: (1) The probe is positioned at some point on a predetermined data acquisition plane using a computer controlled stepper motor system; (2) plasma is pulsed on and allowed to reach a steady state; (3)  $0.5 \mu\text{s}$  before the laser is fired data acquisition begins and continues for 0.32 ms; (4) laser fires; (5) steps (2)–(4) are repeated for five shots (all data presented is a five shot average) at 1 Hz; (6) target is rotated and/or translated; (7) entire process is repeated at a new probe location. Data are acquired using a VXI crate and up to four fast waveform digitizers ( $< 4$  Gsamples/s, 8-bit).

The lpp itself has been analyzed in detailed experiments previously by both this lab and others. Faraday cup measurements in vacuum have shown approximately  $1.5$  and  $2.5 \times 10^{15}$  particles are ablated with an average perpendicular expansion speed of  $v_{\perp}=1.8$  and  $1.4 \times 10^7$  cm/s for carbon and aluminum targets respectively, which corresponds to a kinetic energy about half  $E_{\text{lpp}}$ . These numbers are consistent with experimentally derived scaling laws and previous experiments citing laser to plasma-kinetic energy conversion efficiencies as large as 90% at these laser fluences.<sup>22–24</sup> For our typical background plasma densities of  $2 \times 10^{12} \text{ cm}^{-3}$ , this means that when the lpp has reached the bubble radius it is a factor of  $\approx 10$  more dense than the background. For singly ionized target materials, the directed Larmor radius is always larger than the bubble radius. The order for the relevant speeds is  $c_s \ll v_{\text{lpp}} < v_A \approx v_{te}$ , where for some species  $v_A > v_{te}$  and vice versa. For neon at 500 G,  $v_{\text{lpp}} \approx v_A$ . Here,  $v_A, c_s$ , and  $v_{te}$  are the ambient plasma Alfvén speed, ion-sound speed, and electron thermal speed, respectively.

Shown in the top panel of Fig. 2 is the spatial structure of the measured magnetic field created in the bubble region for carbon lpp expansion into a neon plasma at  $B_o=500$  G

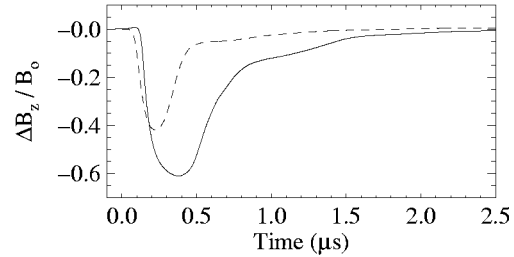
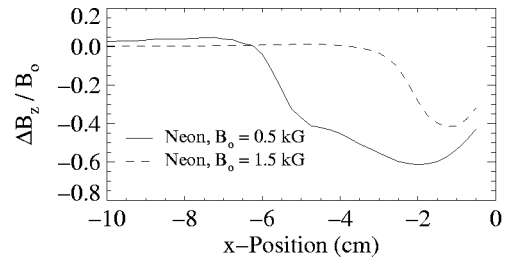


FIG. 2. Diamagnetic cavity. Top panel: The spatial structure of the diamagnetic cavity for a background neon plasma and carbon target with  $B_o=500$  G (solid) and  $B_o=1500$  G (dashed) at time of peak diamagnetism,  $0.41 \mu\text{s}$  and  $0.23 \mu\text{s}$ , respectively. Bottom panel: The received magnetic time signal at  $x=-2$  cm and  $x=-1.25$  cm, for  $B_o=0.5$  kG (solid) and  $B_o=1.5$  kG (dashed), respectively.

and  $B_o=1500$  G at time of peak diamagnetism,  $0.41 \mu\text{s}$  and  $0.23 \mu\text{s}$ , respectively. The temporal structure at the location of the peak signal is shown in the bottom panel of Fig. 2. Each are typical of results obtained previously in experiments at Lawrence Livermore National Laboratory<sup>14</sup> for expansion into vacuum as well the Naval Research Laboratory and Maryland<sup>7,9,10,25</sup> for expansion into gas and photoionized plasma. Several distinct features are apparent in both space and time. The leading edge of the bubble is preceded by a field enhancement which moves at the lpp expansion speed. The cavity center moves initially at the expansion speed but slows to a stop by the time it reaches  $R_b$ . Expansion ceases when the cavity has reached the bubble radius  $R_b$ . Not illustrated in the figure, is that the trailing edge of the cavity stays at the target surface and does not move significantly across the field. The classical magnetic diffusion time  $\tau_{\text{md}}$  is given by  $\tau_{\text{md}} = \mu_o \sigma R_b^2$ , where  $\sigma$  is the plasma conductivity ( $\sigma = 50 \pi^{1/2} e_o^2 (kT_e)^{3/2} / m_e^{1/2} e^2 Z \ln \Lambda$ ). For  $T_e=5$  eV, and a bubble radius of 4.0 cm,  $\tau_{\text{md}}=60 \mu\text{s}$ . The field diffuses back into the cavity rapidly at first then slows to a rate which is closer to the classical diffusion time. Figure 3 is a two-dimensional (2D) plane taken at  $z=-2$  cm with interpoint spacing of  $\Delta x = \Delta y = 0.5$  cm for a background neon plasma at 1.5 kG,  $t=0.38 \mu\text{s}$  and aluminum target. The spatial structure from Fig. 2 is realized here in an  $xy$ -plane. Additional observable features include the asymmetry in the field enhancement region and the roughly circular shape of the diamagnetic cavity—excluding a wedgelike tip. The enhancement region appears only on the leading edge of the expansion and continues to expand across the field at the lpp speed while simultaneously growing wider.

Shown in Fig. 4 is a false-color 10 ns gated imager exposure of the visible light emitted by the expanding aluminum lpp  $0.36 \mu\text{s}$  after laser impact. The gated imager was

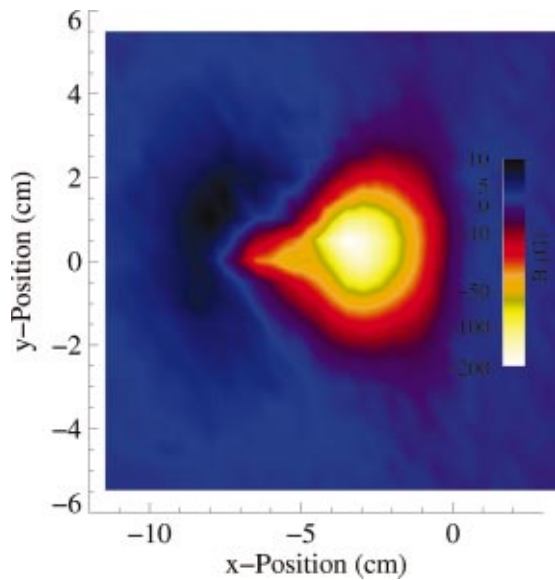


FIG. 3. (Color) 2D plane taken of magnetic field data taken through the diamagnetic cavity for a background neon plasma and aluminum target with  $B_o = 1.5$  kG, at  $z = -2$  cm,  $t = 0.38$   $\mu$ s. The target surface is at  $x = 0$ .

located at  $z = -11$  m with its field of view directed in the  $+\hat{z}$  direction. Overlaid on the image is a vector plot of the perpendicular current density derived from measurements of magnetic field in an  $xy$ -plane at  $z = -2$  cm and  $\mathbf{J} = (1/\mu_o)\nabla \times \mathbf{B}$ . Strictly speaking, there is not enough information to obtain  $\mathbf{J}_\perp = (1/\mu_o)((\partial_y B_z - \partial_z B_y)\hat{x} + (-\partial_x B_z + \partial_z B_x)\hat{y})$ , from measurements made in a plane. However, assuming that the diamagnetic cavity is symmetric about  $z = 0$ , we can derive an approximation for  $\mathbf{J}_\perp$  by neglecting all  $\partial_z$  terms. This figure is unique in that it shows a direct correlation between the visible light emission and the currents responsible for the lpp diamagnetism. In particular, the wedge-like shape of the diamagnetic cavity visible in Fig. 3, is apparent in both the current density and visible light. Previous experiments aimed at understanding lpp cross-field propagation have observed similar structure in the expanding laser-plasma using both resonant imaging techniques as well as fast photography.<sup>26</sup>

To analyze the effect of various background plasmas, the bubble radius as well as the peak change in magnetic field are compared. To derive this from the data, the bubble radius

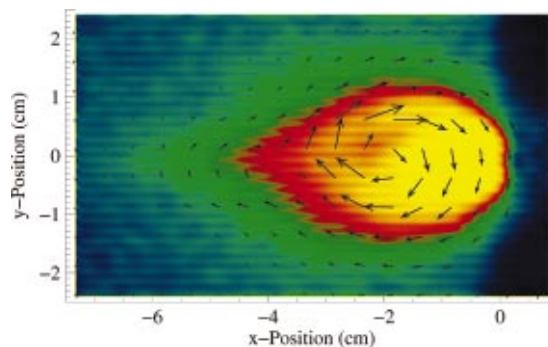


FIG. 4. (Color) False-color 10 ns gated imager exposure with overlaid vectors corresponding to perpendicular current density. Background neon plasma and aluminum target with  $B_o = 1.5$  kG, at  $z = -2$  cm,  $t = 0.36$   $\mu$ s. The target surface is at  $x = 0$ .

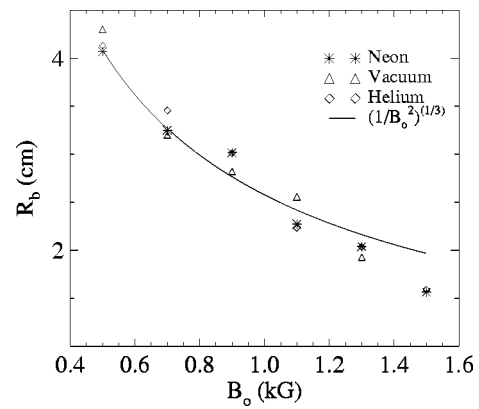


FIG. 5. Experimentally derived bubble radii for carbon lpp expansion into vacuum, neon plasma, and helium plasma. Solid line is expected bubble scaling normalized to the 0.5 kG point.

is calculated by finding the time at which the maximum magnetic energy is expelled from the cavity (peak diamagnetism), then drawing a tangent to the cavity surface at the point of maximum  $|dB/dx|$  ( $dB/dx$  is the spatial derivative of  $B$  with respect to  $x$ -position). The bubble radius is then defined as the distance from the maximum  $|\Delta B_z|$  to the point where the tangent crosses  $B = 0$ . The resulting bubble radii for various background plasmas and magnetic fields are shown in Fig. 5. The solid line is the  $B^{-2/3}$  scaling normalized to the 0.5 kG case. From Fig. 5, it is obvious that the presence of a  $10^{12}$   $\text{cm}^{-3}$  background plasma has a negligible effect on the diamagnetic cavity size. From a pressure standpoint, this is understandable in that at the bubble radius, the lpp is approximately ten times more dense than the background. The radius follows the expected scaling law for all except the highest fields. The depth of the diamagnetic cavity is shown in Fig. 6. As with the bubble radius, the depth of the diamagnetic cavity is not affected by the background plasma. The laser-plasma is less efficient at expelling larger background magnetic fields. At  $B_o = 500$  G,  $\Delta B/B_o \approx 65\%$ , whereas at  $B_o = 1500$  G,  $\Delta B/B_o \approx 42\%$ .

An investigation of the diamagnetic cavity formed by an expanding sub-Alfvénic laser-produced plasma embedded in an ambient magnetized background plasma which can support Alfvén waves has been carried out for a variety of background plasma conditions. Laser plasma diamagnetism [i.e.,

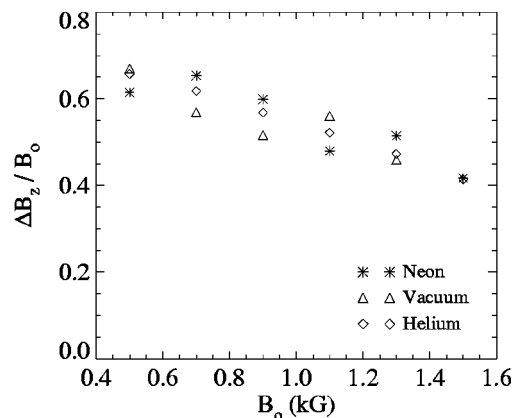


FIG. 6. Experimentally derived bubble depth ( $\Delta B_z/B_o$ ) for carbon lpp expansion into vacuum, neon plasma, and helium plasma.

bubble radius ( $R_b$ ) and cavity depth ( $\Delta B/B$ ) has been observed to be unaffected by the presence of a background plasma which has  $\Delta n/n_o \approx 10$  at  $R_b$ , despite the creation of current structures and shear Alfvén wave radiation in the background plasma.<sup>13,17</sup> For the conditions investigated, it has been shown previously that between 0.5% and 10% of the expanding lpp kinetic energy is radiated into shear Alfvén waves. Recent hybrid simulations have pointed to situations where this number could be increased to 80%–90% of the expanding plasma's kinetic energy<sup>15</sup> with a possible marked effect on the diamagnetic cavity formation. Additionally, for conditions unobtainable in this experiment ( $\Delta n/n_o < 0.01$  at  $R_b$ ) collisions with the background plasma are important and blast wave formation becomes a factor. For these situations, the diamagnetic cavity is severely impacted regardless of Alfvén wave generation.<sup>10</sup>

The diamagnetic cavity size has been found to follow the expected scaling,  $R_b \propto B_o^{-2/3}$  and the cavity depth decreases with increasing magnetic field. At  $B_o = 500$  G,  $\Delta B/B_o \approx 0.65$ , whereas at  $B_o = 1500$  G,  $\Delta B/B_o \approx 0.42$ . In all cases, the background magnetic field diffuses back into the cavity region with two distinct time scales. Each, is faster than that predicted by classical magnetic diffusion. Two-dimensional data-sets have revealed asymmetries in the expanding diamagnetic cavity region which are consistent with visible light images. Specifically, the formation of a jet-like front.

These results may find application to a variety of fields. In inertial confinement fusion research, an ambient magnetized xenon plasma has been proposed as a means for absorbing x-ray radiation as well as slowing the target debris. This research likely shows that for background densities of  $n_o/n_{lpp} \approx 1/10$  at  $R_b$  no significant signature of the background plasma should be observable on the diamagnetic cavity. Additionally, this research shows that visible light emission from expanding high-beta plasmas can be highly correlated with the underlying magnetic structure possibly aiding in the difficult interpretation of optical images.

## ACKNOWLEDGMENTS

The authors gratefully acknowledge the help of R. J. Taylor in obtaining the gated imager photo presented in Fig. 4. The authors wish to thank G. Dimonte for his help with the preliminary experiments and also the discussion of his own laser-plasma experiments and simulation results. We

also acknowledge the advice of G. Dipeso and D. Hewett and thank them for sharing their simulation results with us. Also, we are grateful to M. Drandell for his expert technical assistance.

This work was funded by the Department of Energy (DE-F603-98ER54494) and the Office of Naval Research (N00014-97-1-0167). M.V.Z.'s research was performed under appointment to the Fusion Energy Sciences Fellowship Program administered by Oak Ridge Institute for Science and Education under a contract between the U.S. Department of Energy and the Oak Ridge Associated Universities. This work was performed at the Basic Plasma Science Facility (BAPSF) at UCLA. The BAPSF is funded by NSF and DOE under a cooperative agreement.

<sup>1</sup>J. Gosling, Phys. Fluids B **5**, 2638 (1993).

<sup>2</sup>Series of articles on starfish, J. Geophys. Res. **68** (1963).

<sup>3</sup>A. Glass, J. Vac. Sci. Technol. A **4**, 1098 (1986).

<sup>4</sup>S. Bodner, D. Colombant, J. Gardner *et al.*, Phys. Plasmas **5**, 1901 (1998).

<sup>5</sup>R. Peterson, D. Haynes, I. Golovkin, and G. Moses, Phys. Plasmas **9**, 2287 (2002).

<sup>6</sup>S. Brecht, M. Pesses, J. Lyon, N. T. Gladd, and S. W. McDonald, Geophys. Res. Lett. **22**, 1805 (1995).

<sup>7</sup>S. Kacenjar, M. Hausman, M. Keskinen *et al.*, Phys. Fluids **29**, 2007 (1986).

<sup>8</sup>V. Antonov, V. Bashurin, A. Golubev *et al.*, J. Appl. Mech. Tech. Phys. **26**, 757 (1985).

<sup>9</sup>B. Ripin, E. McLean, C. Manka *et al.*, Phys. Rev. Lett. **59**, 2299 (1987).

<sup>10</sup>B. Ripin, J. Huba, E. McLean *et al.*, Phys. Fluids B **5**, 3491 (1993).

<sup>11</sup>D. Gurnett, R. Anderson, T. Ma *et al.*, J. Geophys. Res. **91**, 10013 (1986).

<sup>12</sup>P. Bernhardt, Phys. Fluids B **4**, 2249 (1992).

<sup>13</sup>M. VanZeeland, S. Vincena, W. Gekelman, and G. Dimonte, Phys. Rev. Lett. **87**, 105001 (2001).

<sup>14</sup>G. Dimonte and L. Wiley, Phys. Rev. Lett. **67**, 1755 (1991).

<sup>15</sup>G. Dimonte, G. Dipeso, and D. Hewett (private communication) and APS-Division of Plasma Physics 2001.

<sup>16</sup>F. Tsung, G. Morales, and J. Leboeuf, Phys. Rev. Lett. **90**, 055004 (2003).

<sup>17</sup>M. VanZeeland, W. Gekelman, S. Vincena, and J. Maggs, Phys. Plasmas **10**, 1243 (2003).

<sup>18</sup>W. Gekelman, M. VanZeeland, S. Vincena, and P. Pribyl, J. Geophys. Res. **108**, 1281 (2003).

<sup>19</sup>S. Drell, H. Foley, and M. Ruderman, J. Geophys. Res. **70**, 3131 (1965).

<sup>20</sup>J. E. Borovsky, Phys. Fluids **30**, 2518 (1987).

<sup>21</sup>W. Gekelman, H. Pfister, Z. Lucky, J. Bamber, D. Leneman, and J. Maggs, Rev. Sci. Instrum. **62**, 2875 (1991).

<sup>22</sup>B. Meyer and G. Thiell, Phys. Fluids **27**, 302 (1984).

<sup>23</sup>B. Ripin, R. Whitlock, F. Young, S. Obenschain, E. McLean, and R. Decoste, Phys. Rev. Lett. **43**, 350 (1979).

<sup>24</sup>J. Grun, R. Decoste, B. Ripin, and J. Gardner, Appl. Phys. Lett. **39**, 545 (1981).

<sup>25</sup>D. Koopman, Phys. Fluids **19**, 670 (1976).

<sup>26</sup>A. Mostovych, B. Ripin, and J. Stamper, Phys. Rev. Lett. **62**, 2837 (1989).